Quaternary Science Reviews 151 (2016) 88–99

Contents lists available at ScienceDirect

Quaternary Science Reviews

journal homepage: www.elsevier.com/locate/quascirev

Droughts in the East Asian summer monsoon margin during the last 6 kyrs: Link to the North Atlantic cooling events

Jiawei Fan [a, b, *], Jule Xiao [a, c], Ruilin Wen [a], Shengrui Zhang [a, b], Xu Wang [a], Linlin Cui [a], He Li [d], Dingshuai Xue [d], Hideki Yamagata [e]

[a] Key Laboratory of Cenozoic Geology and Environment, Institute of Geology and Geophysics, Chinese Academy of Sciences, Beijing 100029, China
[b] University of Chinese Academy of Sciences, Beijing 100049, China
[c] College of Earth Sciences, University of Chinese Academy of Sciences, Beijing 100049, China
[d] State Key Laboratory of Lithospheric Evolution, Institute of Geology and Geophysics, Chinese Academy of Sciences, Beijing 100029, China
[e] Paleo Labo Co., Ltd., Saitama 335–0016, Japan

ARTICLE INFO

Article history:
Received 26 April 2016
Received in revised form
28 August 2016
Accepted 2 September 2016

Keywords:
Dali lake
Endogenic calcites
Elements
Stable isotopes
East Asian summer monsoon
Last 6 kyrs

ABSTRACT

Teleconnections to the high latitudes, forcing by the tropical oceans and solar variability have all been suggested as dominant factors in the sub-millennial global climate changes, yet there is little consensus as to the relative importance of these factors for the East Asian summer monsoon (EASM) variability. This study presents the results of high-resolution analyses of Ca and Mg concentrations, Mg/Ca ratio, $\delta^{18}O$ and $\delta^{13}C$ values of endogenic calcites from a sediment core from Dali Lake in the EASM margin, in order to investigate the sub-millennial EASM variability and its possible driving forces during the last 6 kyrs. Increases in these chemical proxy data were interpreted as drought events in the region due to the intensive evaporation losses overwhelming the water input to the lake. The chemical proxy data in this study combined with multi-proxy indicators including grain size component and total organic carbon concentrations from the same sediment core imply that declines in the EASM intensity may have played a dominant role in triggering the drought events during the last 6 kyrs. The results indicate that the EASM intensity significantly declined at the intervals of 5.8–4.75, 3.2–2.8, 1.65–1.15 and 0.65–0.2 kyrs BP. Large declines in the EASM intensity during the last 6 kyrs correspond in time to occurrences of ice-rafted debris in the North Atlantic, indicating that millennial-to-centennial scale changes in the EASM intensity were mainly controlled by climatic processes occurring in the northern high latitudes. These data imply that persistent global warming may be favorable for the strengthening of the EASM circulation and for the transportation of more rainfall to the semi-arid regions of northern China on sub-millennial scales.

1. Introduction

The East Asian summer monsoon (EASM) is an integral component of the global climate system, and plays a key role in transporting heat and moisture from low to high latitudes (An, 2000). On the regional scale, the large variability of the EASM can cause calamitous flooding or severe drought that impacts more than a quarter of the world's population. In recent years, more and more attention has been paid to the effect of future global warming on the EASM (IPCC, 2013). However, there is little consensus as to this highly contested issue because the dominant factors forcing the variability of the EASM at sub-millennial time scales are still unclear (Held and Soden, 2006; Li et al., 2010; Broecker and Putnam, 2013).

Several studies indicated that solar variability was the main cause of global climate change at centennial time scales (Stuiver, 1980; Yu and Ito, 1999; Staubwasser et al., 2003). Solar forcing could change the position of polar front and subtropical jets through its influence on the stratospheric ozone and temperature (Shindell et al., 2001). However, several other studies argued that there was no significant relationship between the paleoclimatic records in tropical low latitudes and the atmospheric $\Delta^{14}C$ records (Russell et al., 2003; Russell and Johnson, 2005), which partly reflect the solar variability (Stuiver, 1980). These studies suggested

* Corresponding author. Key Laboratory of Cenozoic Geology and Environment, Institute of Geology and Geophysics, Chinese Academy of Sciences, Beijing 100029, China.
E-mail address: jwfan@mail.iggcas.ac.cn (J. Fan).

http://dx.doi.org/10.1016/j.quascirev.2016.09.001
0277-3791/

that the variability within the tropical oceans may be the dominant forcing of global climate change. Camberlin et al. (2001) found that changes in tropical Pacific sea surface temperatures during modern El Niño events could exert a direct influence on equatorial African rainfall through changes in atmospheric and oceanic circulation in Indian and Atlantic Oceans. Nelson et al. (2011) suggested that changes in the El Niño Southern Oscillation in the tropical Pacific could have a great impact on the precipitation variability in the Pacific Northwest. In addition, some studies suggested that the significant sub-millennial cooling events that occurred in the North Atlantic during the Holocene could have global impacts (Bond et al., 2001). General circulation models pointed out that cooling in the North Atlantic could cause anomalous Atlantic trade winds and cross-equatorial moisture transport, thereby shifting the Inter-tropical Convergence Zone southward (Vellinga and Wood, 2002; Lohmann, 2003) and leading to significant decreases in the precipitation in the northern subtropics (Wang et al., 2005, 2008; Chen et al., 2016). Despite mounting evidence for these factors affecting the global climate, the relative importance among them is still a controversial issue. Therefore high-resolution, well-dated paleoclimatic records from middle latitude regions are needed to be compared with the climatic processes in high and low latitudes, in order to detect the dominant factors controlling the regional climate change.

Dali Lake is located at the transition from semi-humid to semi-arid regions in the northern middle latitudes, where the regional precipitation is mainly controlled by the EASM (An, 2000). Endogenic carbonates precipitated in lakes in semi-arid regions can provide direct information on past changes in the regional climate (Talbot and Allen, 1996). This study presents ~50-yr resolution records of elements and stable isotopes of endogenic calcites from the Dali Lake sediments in order to reconstruct a prominent feature of the EASM variability during the last 6 kyrs, and improve our understanding of the dominant driving forces of the EASM variability. These data would provide insights into how the EASM may respond to the global warming in the future.

2. Regional setting

Dali Lake (43°13′–43°23′ N, 116°29′–116°45′ E) is located in the northern margin of the E–W-extending Hulandaga Desert Land, 70 km west of Hexigten Banner, Inner Mongolia (Fig. 1), in an inland fault-depression basin that was formed in the Pliocene to Pleistocene (Li, 1993). The lake has an area of 238 km^2, a maximum water depth of 11 m, an elevation of 1226 m above sea level (Fig. 1), and is hydrologically closed. Hills surround the lake to the north and west, and lacustrine plains are present along the eastern shore. Two permanent rivers, the Gongger and Salin Rivers, enter the lake from the northeast and two intermittent streams, the Holai and Liangzi Rivers, enter from the southwest (Fig. 1); however, there are no outflowing rivers. The Gongger River, the major inflow, rises in the southern terminal part of the Great Hinggan Mountains, where the elevation reaches 2029 m, and has a drainage area of 783 km^2 and a total channel length of 120 km (Li, 1993). Hydrological observations indicate that the discharge of the Gongger River is as large during spring floods in April as during summer floods in July, because of significant melt water runoff from the snow/ice packs covering the mountains (Li, 1993).

Dali Lake is located at the transition from semi-humid to semi-arid regions of the middle temperate zone. The climate of the region is mainly controlled by the East Asian monsoon (An, 2000). In region, mean annual temperature is 3.2 °C with a July average of 20.4 °C and a January average of −16.6 °C (Fig. 2). Mean annual precipitation is 383 mm, and ~70% of the annual precipitation falls from June–August (Fig. 2). Mean annual evaporation reaches 1632 mm, which is more than 4 times the annual precipitation (Fig. 2). The lake is covered with ice from early November to late April (Li, 1993).

3. Materials and methods

3.1. Water sampling and hydrochemical analyses

Water in the Dali Lake was sampled using a PURITY stainless steel depth-setting water sampler (Model WB-SS) from the central-northwestern, central-northeastern and central-southern parts of the lake in June 2010, while water from the four inflowing rivers was sampled in April and August 2011, respectively. Temperature and pH measurements were taken on site using a HANNA portable multi-parameter water quality analyzer (Model HI9828). Ion concentrations and isotope composition were measured in laboratory. Concentrations of major cations of Ca^{2+}, Mg^{2+}, K^+ and Na^+ in the water were determined with an IRIS Intrepid II XSIP Inductively Coupled Plasma Optical Emission Spectrometer (ICP-OES), and the relative standard deviation was less than 5%. Concentrations of anions of SO_4^{2-} and Cl^- were determined with an ICS-1000 Ion Chromatograph Spectrometer, and the relative standard deviation was less than 5%. In addition, concentrations of CO_3^{2-} and HCO_3^- were determined by titration, and the repeated measurement error was less than 1%. Water salinities were calculated by using the sum of total major ion (Ca^{2+}, Mg^{2+}, K^+, Na^+, and CO_3^{2-}, HCO_3^-, SO_4^{2-}, Cl^-) concentrations, while alkalinities were calculated by the sum of CO_3^{2-} and HCO_3^- concentrations and expressed in $CaCO_3$ g/L. The $\delta^{18}O$ (VSMOW) values of the water and the $\delta^{13}C$ values of the water's dissolved inorganic carbon ($\delta^{13}C_{DIC}$) (PDB) were determined with a Finnigan Delta S Mass Spectrometer, and the precision was better than 0.1‰ for both $\delta^{18}O$ and $\delta^{13}C_{DIC}$ values. The δ^2H (δD) (VSMOW) values were determined with a Finnigan MAT 252 Mass Spectrometer, and the precision was better than 1‰.

3.2. Sediment sampling and lithology

Sediment coring was conducted at a water depth of 10.8 m in the depocenter of Dali Lake in February 2004, when the lake surface was frozen (Fig. 1), using a TOHO drilling system (Model D1-B) (Toho Chikakoki Co., Ltd, Japan). Incremental sediment cores were extracted to a total depth of 11.83 m beneath the lake floor and were designated DL04 (43°15.68′ N, 116°36.26′ E) (Fig. 1). The cores were collected in polyethylene tubes using a piston corer of the drilling system, and sediment recovery was close to 100%. All of the sediment cores were split, photographed and described on site, and then cut into 1-cm segments for samples. There was no indication of any sedimentary hiatuses (Fig. 3).

The upper 6.39 m of the DL04 core was used for the present study (Fig. 3). The sediments of the upper 6.39 m were composed of homogeneous clayey silt and silt, and could be divided into four main sedimentary units (Fig. 3), as follows: 6.39–6.34 m greenish-grey massive silt with occasional blackish-grey bands; 6.34–5.98 m blackish-grey banded clayey silt; 5.98–4.94 m greenish-grey laminated clayey silt; 4.94–0 m blackish-grey massive clayey silt. $CaCO_3$ contents in the sediments of the upper 6.39 m of the DL04 core were generally higher than 10% with an average of 20% and a maximum of 41%. Below the core depth of 6.39 m, the $CaCO_3$ contents were close to zero in most horizons (Fig. 3). The upper 6.39 m of the DL04 core was sampled at 3- to 6-cm intervals, yielding a total of 114 samples for laboratory analyses.

3.3. Radiocarbon dating

Eleven bulk samples were collected at 50- or 100-cm intervals

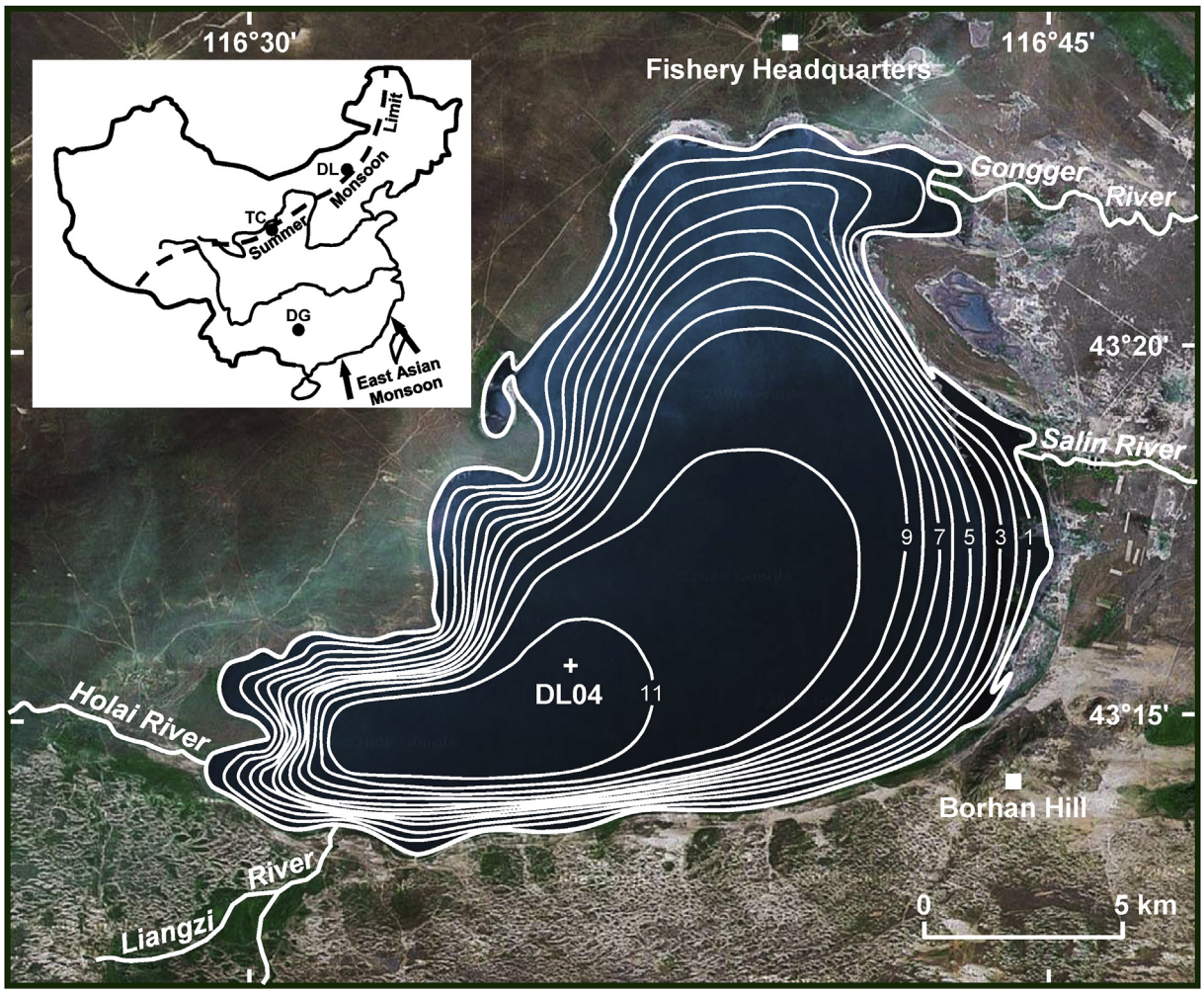

Fig. 1. Map of Dali Lake (from http://maps.google.com) showing the location of the DL04 sediment core (cross). The bathymetric survey of the lake was conducted in June 2002 using a FE-606 Furuno Echo Sounder (contours in m). The inset map shows the locations of Dali Lake (DL) (43°15.68′ N, 116°36.26′ E), Tianchi Lake (TC) (35°15.88′ N, 106°18.55′ E) (Zhao et al., 2010) and Dongge Cave (DG) (25°17′ N, 108°5′ E) (Wang et al., 2005) in China (solid circles) and the modern northern limit of the East Asian summer monsoon defined by the 400-mm isohyet of mean annual precipitation.

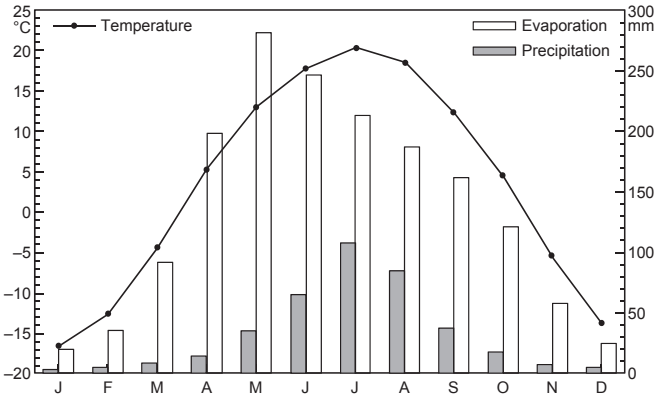

Fig. 2. Mean monthly temperature, mean monthly precipitation and mean monthly evaporation in the Dali Lake region. Data are the average of observations from 1981 to 2010 at Hexigten Banner Meteorological Station, 70 km east of Dali Lake (unpublished data courtesy of Inner Mongolia Meteorological Bureau).

from the organic-rich horizons of the upper 6.5 m of the DL04 core for radiocarbon dating (Fig. 3; Table 1). Samples were dated with an Accelerator Mass Spectrometry (AMS) system (Compact-AMS, NEC Pelletron) at the Paleo Labo Co., Ltd (Japan) (Xiao et al., 2008). Bulk organic matter was extracted from each sample and dated following the method described by Nakamura et al. (2000). The $^{14}C/^{12}C$ and $^{13}C/^{12}C$ ratios of each sample, with an oxalic acid standard (SRM-4990C, commonly designated HOxII), were measured with a HVEE AMS system. Each sample was measured three times, and each measurement lasted 30 min: The typical uncertainty due to counting statistics was 0.3%. In order to correct the $^{14}C/^{12}C$ ratios for isotopic fractionation, the $\delta^{13}C$ value of each sample was analyzed with a conventional multi-collector mass spectrometer. The background level of the AMS system measured by pure graphite powder is between 50 and 55 kyrs BP (Nakamura et al., 2000).

The ^{14}C dates of all the samples were determined with a half-life of 5568 yr (Table 1). As shown in Table 1, the uppermost 1 cm of the DL04 core yielded a ^{14}C age of 472 yr. This anomalously old age could be considered to result from reservoir effects on radiocarbon dating of the Dali Lake sediments. In order to produce an age–depth model for the upper 6.5 m of the DL04 core, the reservoir age of 472 yr was first subtracted from all the original ^{14}C ages, assuming a constant offset throughout the core. The conventional ages were then converted to calibrated ages using the OxCal4.2 radiocarbon age calibration program (Bronk Ramsey and Lee, 2013) with IntCal13 calibration data (Reimer et al., 2013).

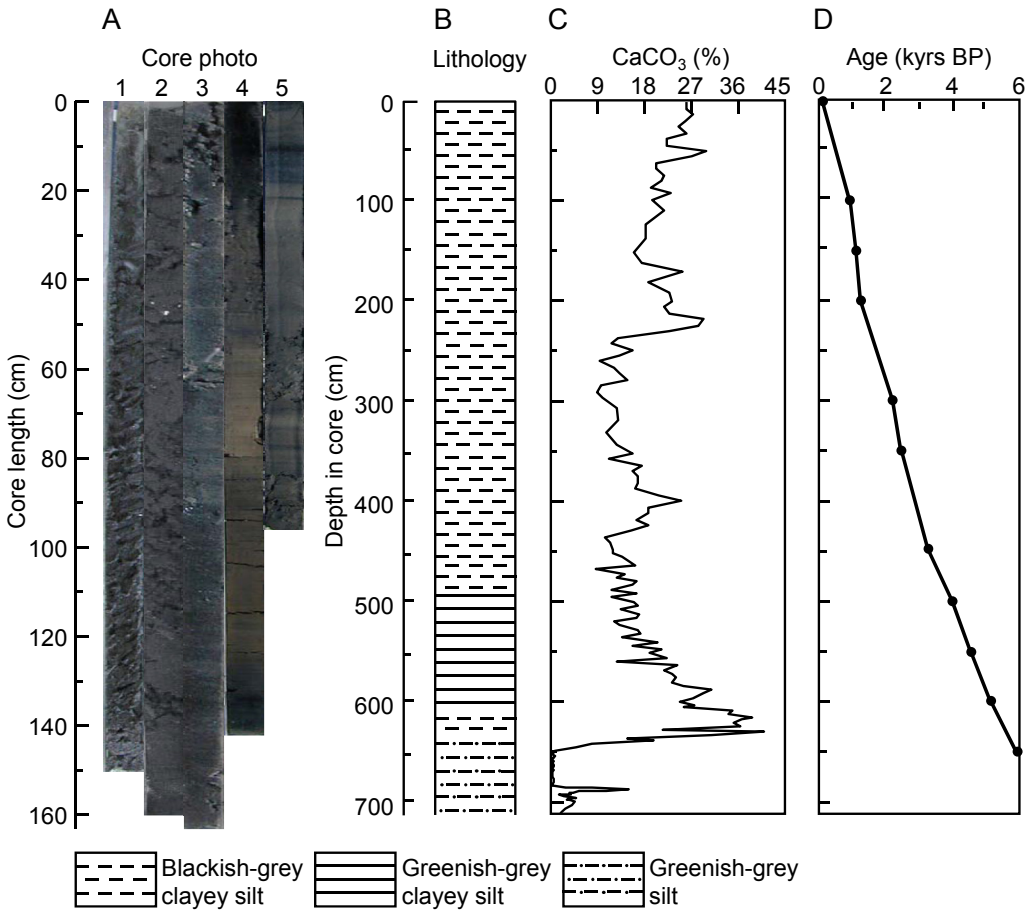

Fig. 3. (A) Photograph of the upper 7.11 m of the DL04 core. The 1st section is the interval 0–150 cm, and the 5th section is the interval 615–711 cm. (B) Lithology of the upper 7.11 m of the DL04 core. (C) $CaCO_3$ content in bulk samples from the upper 7.11 m of the DL04 core, calculated by the content of total inorganic carbon in bulk samples (Xiao et al., 2008) times a coefficient of 8.33. (D) Age–depth model of the upper 6.5 m of the DL04 core. Dots represent the mean values of 2σ ranges of calibrated ages of reservoir-corrected radiocarbon dates.

Table 1
AMS radiocarbon dates of samples from the upper 6.5 m of the DL04 core.

Laboratory number[a]	Depth interval (cm)	Dating material	$\delta^{13}C$ (‰)	^{14}C age (^{14}C yr BP)	Corrected ^{14}C age[b] (^{14}C yr BP)	Calibrated ^{14}C age (2σ) (cal yr BP)
PLD–4564	1–0	Organic matter	−28.19	472 ± 23	0 ± 33	74–32
PLD–4565	100–99	Organic matter	−25.47	1463 ± 24	991 ± 33	965–892
PLD–6250	150–149	Organic matter	−28.05	1629 ± 22	1157 ± 32	1176–982
PLD–4567	200–199	Organic matter	−24.65	1948 ± 25	1476 ± 34	1415–1300
PLD–12450	299–298	Organic matter	−23.24	2652 ± 22	2180 ± 32	2313–2114
PLD–12453	350–349	Organic matter	−24.60	2879 ± 23	2407 ± 33	2503–2347
PLD–12456	449–448	Organic matter	−25.36	3561 ± 24	3089 ± 33	3376–3217
PLD–12459	500–499	Organic matter	−27.80	4113 ± 25	3641 ± 34	4013–3865
PLD–6706	550–549	Organic matter	−23.66	4562 ± 21	4090 ± 31	4654–4516
PLD–4572	600–599	Organic matter	−27.24	4947 ± 28	4475 ± 36	5292–5031
PLD–6255	650–649	Organic matter	−25.58	5709 ± 26	5237 ± 35	6029–5917

[a] PLD: Paleo Labo Dating, laboratory code of Paleo Labo Co., Ltd., Japan.
^{14}C age of the uppermost 1 cm of the DL04 core.
[b] The reservoir correction factor is 472 yr.

The age–depth model of the DL04 core was created by linear interpolation between radiocarbon-dated horizons using the mean values of 2σ ranges of calibrated ages, and the upper 6.5 m of the DL04 core covered the last 6 kyrs (Fig. 3; Table 1). The sedimentation rates of ca. 60–280 cm/kyr for the upper 6.5 m of the DL04 core and sampling intervals of 3–6 cm in the present study provided potential temporal resolutions of ca. 40–60 yr for the geochemical data.

3.4. Geochemical analyses

The sediments <38 μm in grain size were sieved from each of 114 samples from the upper 6.39 m of the DL04 core for analyses of Ca and Mg concentrations, Mg/Ca ratio, and oxygen and carbon isotope composition of the carbonates. Each sample of ca. 500 mg of air-dried bulk sediments was fully ground with a ceramic mortar

Table 2
Chemical characteristics of water samples from Dali Lake and the inflowing rivers.

Water sample	pH	T (°C)	Salinity (g/L)	Alkalinity ($CaCO_3$ g/L)	Ca^{2+} (mg/L)	Mg^{2+} (mg/L)	K^+ (mg/L)	Na^+ (mg/L)	CO_3^{2-} (mg/L)	HCO_3^- (mg/L)	SO_4^{2-} (mg/L)	Cl^- (mg/L)	$\delta^{18}O$ (‰)	δD (‰)	$\delta^{13}C_{DIC}$ (‰)
Dali Lake[a]	9.3	16.0	9.2	5.0	7.2	50.2	410.0	3120.0	643.0	2415.0	388.0	1710.0	−2.1	−20.3	−0.2
Dali Lake[b]	9.6	17.3	7.5	4.7	4.7	21.6	152.0	2360.0	622.0	2253.0	396.0	1740.0	−2.2	−24.3	−0.7
Dali Lake[c]	9.6	14.1	5.5	4.9	4.7	29.4	237.0	2070.0	668.0	2340.0	425.0	1810.0	−2.1	−22.8	−0.1
Gongger River[d]	8.3	0.6	0.2	0.2	18.8	6.3	2.6	18.4	0	135.2	15.4	8.5	−15.3	−108.0	−6.3
Gongger River[e]	8.7	21.6	0.2	0.2	30.0	8.4	2.6	16.6	6.1	126.6	7.1	6.5	−10.8	−80.9	−9.3
Salin River[d]	9.0	10.5	0.5	0.5	21.2	25.5	8.1	62.1	12.4	290.9	10.2	24.5	−4.6	−42.1	2.5
Salin River[e]	7.9	21.0	0.4	0.4	21.2	23.1	10.8	55.8	0	256.2	9.2	20.4	−3.4	−36.6	−2.0
Liangzi River[d]	8.1	0.5	0.2	0.2	15.1	7.2	1.8	15.4	0	138.4	5.1	4.6	−10.1	−71.7	−6.2
Liangzi River[e]	7.4	15.7	0.2	0.2	30.6	9.4	4.1	15.8	0	151.2	5.9	5.1	−10.2	−71.8	−9.7
Holai River[d]	8.5	1.9	0.3	0.3	17.2	13.3	2.1	25.0	0	188.7	11.6	8.0	−9.2	−74.7	−7.6
Holai River[e]	7.9	14.1	0.3	0.4	36.5	17.5	5.1	23.9	0	219.2	12.8	8.8	−10.2	−69.8	−10.5

[a, b, c] Sampled in June 2010 from the central-northwestern, central-northeastern and central-southern parts of the lake.
[d]Sampled during spring floods in April 2011.
[e]Sampled during summer floods in August 2011.

and a rubber-sheathed pestle. The ground sediments were sieved through a 400-mesh (38-μm pore size) sieve to obtain the <38-μm sediments for each sample.

Concentrations of Ca and Mg of the carbonates in <38-μm sediments were determined with an ICP-OES. Each sample of 100 mg of <38-μm sediments was pre-treated with 40 ml of deionized water with a full stirring, and the sample solution was centrifuged to remove absorbed Ca and Mg. 40 ml of 1% acetic acid was added to the resulting residue, and the solution was kept for reaction for 10 min to dissolve carbonates. The solution was then centrifuged at 3000 rpm for 5 min to obtain the supernatant solution (acetic acid solution) that was diluted 1000 times with nitric acid solution for measurements of Ca and Mg concentrations. Multi-element standards prepared by acetic acid dilution of GSB mono-element nitric acid standard solutions (GSB041720 for Ca; GSB041735 for Mg) for ICP-OES were used for calibration of the measured values of Ca and Mg concentrations. Ca and Mg were determined, and their concentrations were calculated with the wavelength and intensity of the characteristic spectrum. The relative error was less than 5% for both Ca and Mg concentrations. Ca and Mg concentrations were expressed in weight percentages in <38-μm sediments of a sample. In addition, Mg/Ca mole ratio was calculated by its mass ratio times a coefficient of 1.67.

$\delta^{18}O$ and $\delta^{13}C$ values of the <38-μm carbonates were determined with a Finnigan MAT 253 mass spectrometer equipped with a Gas Bench−II carbonate preparation device. Each sample of 2−5 mg of <38-μm sediments was added by 50 μl of 103% H_3PO_4, and the sample solution was kept for reaction in Gas Bench−II at 72 °C for 1 h to generate an appropriate amount of CO_2 for measurements of $^{18}O/^{16}O$ and $^{13}C/^{12}C$ ratios. A reference carbonate sample, IVA, was routinely analyzed after every six-sample measurements. $\delta^{18}O$ and $\delta^{13}C$ values were expressed in parts per thousand (‰) relative to VPDB. All $\delta^{18}O$ and $\delta^{13}C$ values were normalized to IVA, the certified $\delta^{18}O$ and $\delta^{13}C$ values of which were −1.90‰ and 2.21‰, respectively. The precision was better than 0.1‰ for both $\delta^{18}O$ and $\delta^{13}C$ values.

3.5. Numerical analyses

In order to detect the pattern of temporal changes in the regional environment during the last 6 kyrs, principle component analysis (PCA) was performed using the software SPSS to analyze the time series of data of Ca and Mg concentrations, Mg/Ca ratio and $\delta^{18}O$ and $\delta^{13}C$ values. All the raw data of the geochemical proxies were standardized, and then PCA was conducted on the standardized data with the proxies as variables. The main factors of PCA were selected according to the criterion of the accumulative total variance higher than 85%. The eigenvector between each of the main factors and its corresponding variable was determined by the ratio of the main factor's loadings to the square root of its total eigenvalue. The value of each of the main factors was calculated by the product of its eigenvector and the standardized data.

4. Results

The water of Dali Lake at present has an average pH value of 9.5, an average salinity of 7.4 g/L and an average alkalinity of 4.9 $CaCO_3$ g/L (Table 2). The lake water contains major cations (average values) of Ca^{2+} (5.5 mg/L), Mg^{2+} (33.7 mg/L), K^+ (266.3 mg/L) and Na^+ (2516.7 mg/L), and major anions (average values) of CO_3^{2-} (644.3 mg/L), HCO_3^- (2336.0 mg/L), SO_4^{2-} (403.0 mg/L) and Cl^- (1753.3 mg/L). The Mg/Ca mole ratio of lake water averages 8.3. The $\delta^{18}O$ and δ^2H values of lake water average −2.1‰ and −22.5‰, respectively, while the $\delta^{13}C_{DIC}$

averages −0.3‰ (Table 2). Data of chemical properties of water sampled from the inflowing rivers to the lake are shown in Table 2.

Ca and Mg concentrations, Mg/Ca ratio, $\delta^{18}O$ and $\delta^{13}C$ and PCA F1 values are plotted against calibrated age in Fig. 4. Overall, temporal changes in the five geochemical proxies are characterized by 4 intervals at which the proxies exhibit significant increases in their values. These intervals include 5.8–4.75, 3.2–2.8, 1.65–1.15 and 0.65–0.2 kyrs BP, respectively (Table 3). The averages of Ca and Mg concentrations, Mg/Ca ratios, and $\delta^{18}O$ and $\delta^{13}C$ values for the last 6 kyrs are 2.71%, 0.53%, 0.33, −4.08‰ and 1.5‰, respectively. At 5.8–4.75 kyrs BP, Ca and Mg concentrations and Mg/Ca ratios average 2.94%, 0.6% and 0.34 with high peaks of 3.1%, 0.67% and 0.37, respectively; while $\delta^{13}C$ values average 3.03‰ with a high peak of 3.43‰. At 3.2–2.8 kyrs BP, Ca and Mg concentrations and Mg/Ca ratios average 2.76%, 0.55% and 0.33 with high peaks of 2.87%, 0.57% and 0.35, respectively; while $\delta^{18}O$ and $\delta^{13}C$ values average −3.71‰ and 2.03‰ with high peaks of −3.28‰ and 2.53‰. At 1.65–1.15 kyrs BP, Ca and Mg concentrations and Mg/Ca ratios average 2.85%, 0.59% and 0.34 with high peaks of 2.99%, 0.64% and 0.36, respectively; while $\delta^{18}O$ and $\delta^{13}C$ values average −3.43‰ and 1.57‰ with high peaks of −2.01‰ and 3.18‰. At 0.65–0.2 kyrs BP, Ca and Mg concentrations and Mg/Ca ratios average 2.67%, 0.58% and 0.36 with high peaks of 2.79%, 0.62% and 0.39, respectively; while $\delta^{18}O$ and $\delta^{13}C$ values average −3.05‰ and 1.32‰ with high peaks of −2.76‰ and 1.47‰. It is notable that $\delta^{18}O$ maintains its lowest values of the last 6 kyrs at 5.8–4.75 kyrs BP and exhibits a minimum of as low as −6.11‰.

PCA F1, F2 and the first three factors capture 51.7%, 22.8% and 94.5% of the total variance within the data set, respectively (Fig. 5). The average of PCA F1 values for the last 6 kyrs is close to 0. At these 4 intervals, the PCA F1 values average 2.04, 0.68, 1.34 and 1.14, respectively (Table 3); with maximums of 3.17, 1.51, 2.53 and 2.21, respectively. In addition, in the PCA ordination diagram the vector of $\delta^{18}O$ values deviated significantly from the PCA F1 axis (Fig. 5), which may be resulted from the anomalously low $\delta^{18}O$ values at the interval of 5.8–4.75 kyrs BP. These data indicate that PCA F1 could reflect the common characteristics of the data of Ca and Mg concentrations, Mg/Ca ratio, $\delta^{18}O$ and $\delta^{13}C$ values.

5. Discussion

5.1. Paleoenvironmental interpretation of the geochemical proxies

Previous studies suggested that carbonates precipitated in lake

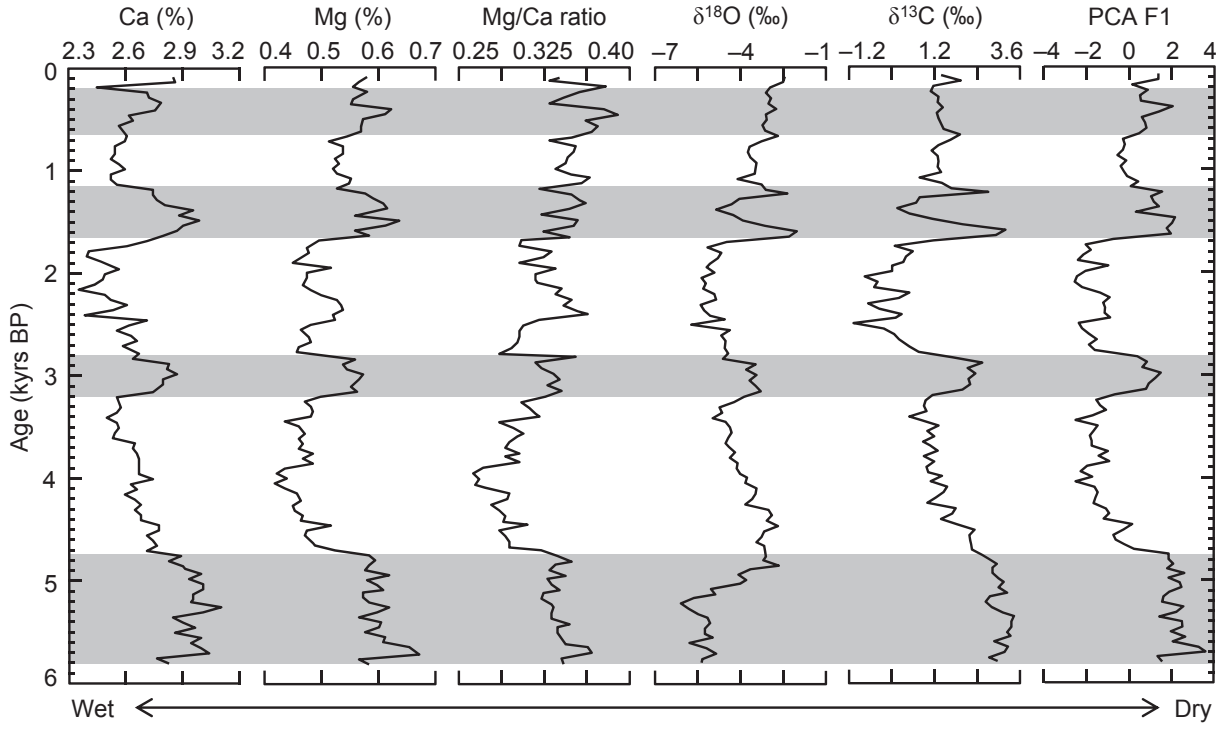

Fig. 4. Time series of Ca and Mg concentrations, Mg/Ca mole ratio and $\delta^{18}O$ and $\delta^{13}C$ values of <38-μm calcites from the DL04 core as well as PCA F1 value obtained from data of the five geochemical proxies spanning the last 6 kyrs. Ca and Mg concentrations are expressed in weight percentages in <38-μm sediments of a sample. PCA F1, F2 and F3 factors capture 51.7%, 22.8% and 20.0% of the total variance within the data set, respectively. The chronology is derived from the carbon reservoir-corrected age–depth model. Shaded bars mark the intervals of strong evaporation of the lake water and dry climate in the region.

Table 3
The averages of geochemical data of <38-μm calcites from the DL04 core as well as the averages of PCA F1 values obtained from the geochemical data at the intervals of 5.8–0, 5.8–4.75, 3.2–2.8, 1.65–1.15 and 0.65–0.2 kyrs BP, respectively.

Intervals (kyrs BP)	Ca (%)	Mg (%)	Mg/Ca ratio	$\delta^{18}O$ (‰)	$\delta^{13}C$ (‰)	PCA F1
0.65–0.2	2.67	0.58	0.36	−3.05	1.32	1.14
1.65–1.15	2.85	0.59	0.34	−3.43	1.57	1.34
3.2–2.8	2.76	0.55	0.33	−3.71	2.03	0.68
5.8–4.75	2.94	0.60	0.34	−4.77	3.03	2.04
5.8–0	2.71	0.53	0.33	−4.08	1.50	0

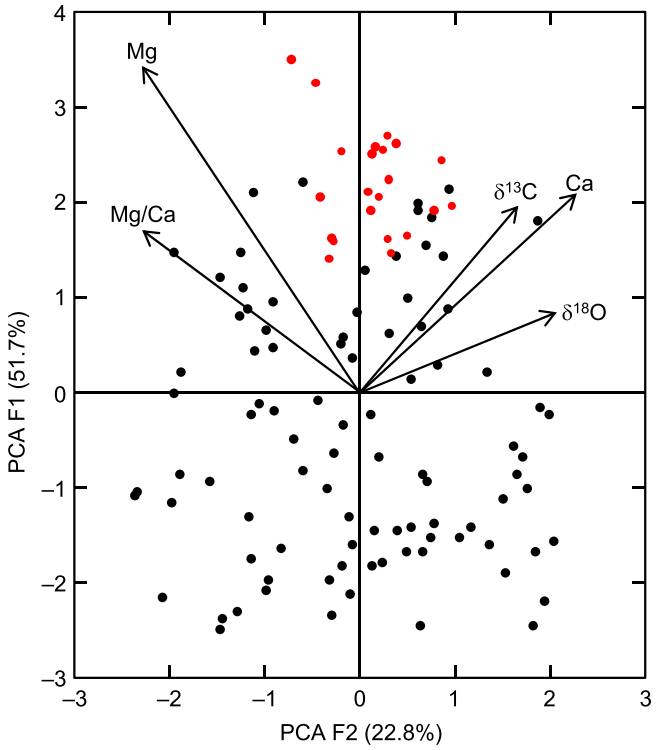

Fig. 5. PCA ordination of the data of Ca and Mg concentrations, Mg/Ca mole ratio and $\delta^{18}O$ and $\delta^{13}C$ values of <38-μm calcites from the DL04 core spanning the last 6 kyrs. PCA F1 and F2 factors capture 51.7% and 22.8% of the total variance within the data set, respectively. The red circles represent the data at the interval of 5.8–4.75 kyrs BP and the arrows represent the vectors instead of eigenvectors of the five chemical proxies. (For interpretation of the references to colour in this figure legend, the reader is referred to the web version of this article.)

water, i.e., endogenic carbonates, were commonly finer in grain size than sands (Lerman, 1978). Different size-fractions of <63, <45, <40 and < 38 μm were used to constrain endogenic carbonate particles separated from the bulk sediments of different lakes (Gu et al., 1993; Fontes et al., 1996; Russell et al., 2003; Qiang et al., 2005; Jiang and Liu, 2007; Steinman et al., 2016). In this study, the <38-μm fraction was selected, and carbonates in the <38-μm sediments were analyzed for Ca and Mg concentrations and stable isotope composition. The Dali Lake basin is surrounded by hills of basaltic rocks to the west, north and east (Li, 1993) and by mobile sand dunes to the south, which implies that detrital carbonates transported from the lake catchment should be negligible in the <38-μm fraction of the lake sediments. X-ray diffraction analyses show that carbonates in the <38-μm sediments of the upper 6.39 m of the DL04 core occur mainly as calcite, with the presence of Mg-calcite in some horizons at core depths of 6.39–6.17 m (5.8–5.4 kyrs BP). Scanning electron microscope (SEM) images of the <38-μm sediments from two representative samples from the upper 6.39 m of the DL04 core exhibit small (1–4 μm) and granular, blocky, lenticular and prismatic idiomorphic carbonate crystals (Fig. 6), indicating that the carbonate crystals were endogenous origin and rapidly precipitated. In addition, calcite in the <38-μm fraction of the surface sediments of Dali Lake has a $\delta^{18}O$ value of −2.5‰ (VPDB), and the modern lake water of −2.1‰ (VSMOW) (Table 2), based on the palaeotemperature equation for the equilibrium precipitation of calcite in lake water re-expressed by Leng and Marshall (2004) as follows:

$$T(^{\circ}C) = 13.8 - 4.58(\delta c - \delta w) + 0.08(\delta c - \delta w)^2$$

where δc is the $\delta^{18}O$ value of calcite with the protocol of VPDB, and δw is the $\delta^{18}O$ value of lake water with the protocol of VSMOW.

The calculated temperature of the lake water is 15.6 °C, which is very close to the measured average value of 15.8 °C (Table 2), supporting that the calcite in the Dali Lake sediments was mainly endogenous origin and precipitated in the lake under the approximate equilibrium of isotopic fractionation (Leng and Marshall, 2004; Liu et al., 2009).

The precipitation of carbonates within hydrologically closed lakes in the semi-arid regions is essentially controlled by the evaporative losses of lake water (Lerman, 1979; Talbot and Allen, 1996; Ito and Forester, 2009). In the semi-arid regions, lake water is usually saturated with respect to $CaCO_3$ because of strong evaporation and low precipitation, so that Ca in lake water is preferentially precipitated as calcite. With the evaporation intensifying, Mg is progressively enriched in lake water, and is incorporated into calcite to form Mg-calcite when the Mg/Ca ratio of lake water exceeds 2 (Müller et al., 1972; Eugster and Jones, 1979; Ito and Forester, 2009). Ca and Mg concentrations in Dali Lake are much lower than other major ions (Table 2), denoting that the strong evaporation of the lake water led to the super-saturation of

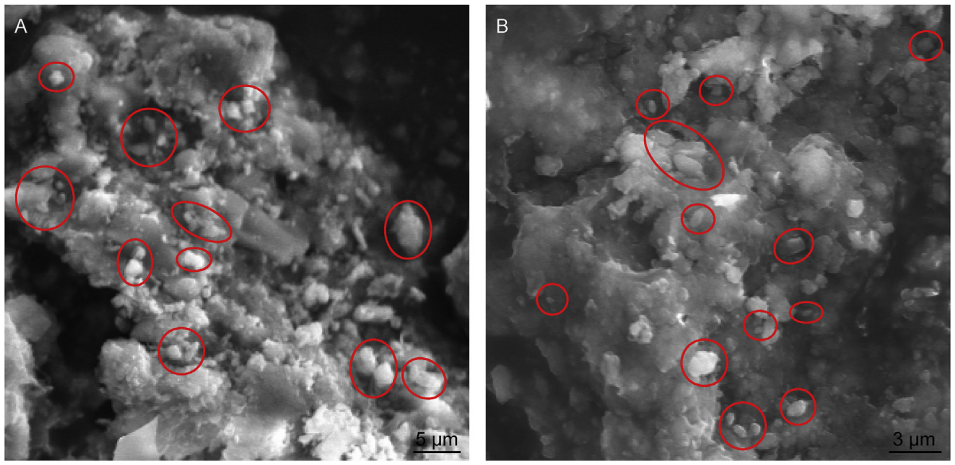

Fig. 6. Scanning electron microscope (SEM) images of the <38-μm sediments from two representative samples at the depths of (A) 2.17 m (1.5 kyrs BP) and (B) 6.32 m (5.68 kyrs BP) from the upper 6.39 m of the DL04 core. The carbonate crystals are marked by red circles. (For interpretation of the references to colour in this figure legend, the reader is referred to the web version of this article.)

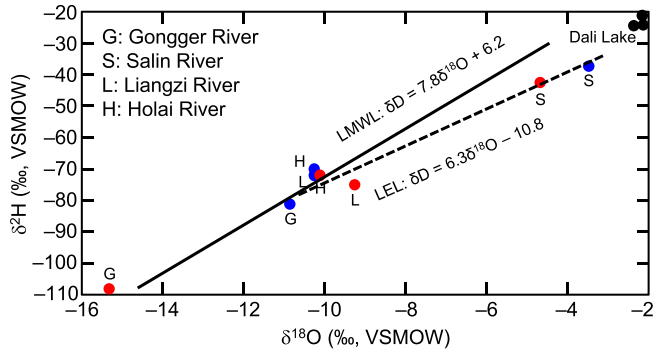

Fig. 7. Isotopic characteristics of water samples from Dali Lake and the inflowing rivers. Solid line represents the local meteoric water line (LMWL) calculated from the isotopic data from Shihua Cave station (39°47′ N, 115°56′ E) in Beijing (Li et al., 2015) which is the closest station to the Dali Lake region in the monsoonal region. Dashed line represents the local evaporation line (LEL) calculated from the isotopic data from the water samples from Dali Lake and the inflowing rivers. Black dots show isotope values of the lake water. Blue and red dots show isotope values of the river water in summer and winter, respectively. See Fig. 1 for locations of the inflowing rivers, Gongger, Salin, Liangzi and Holai. (For interpretation of the references to colour in this figure legend, the reader is referred to the web version of this article.)

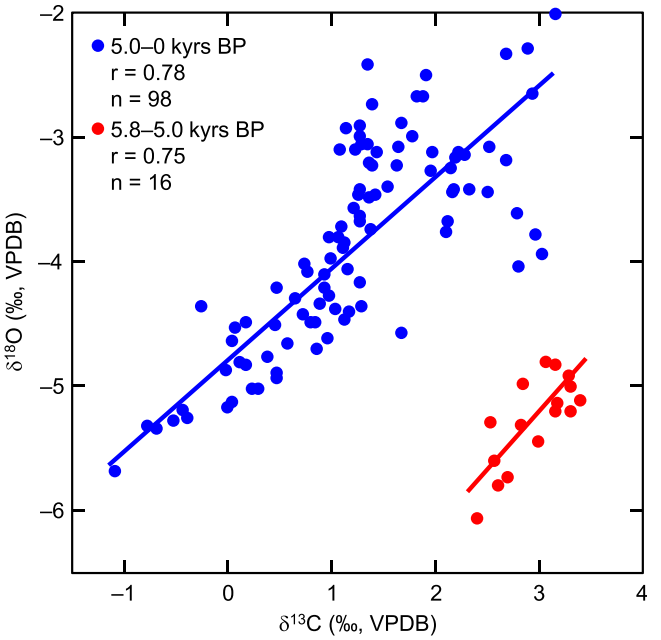

Fig. 8. Relationship between $\delta^{18}O$ and $\delta^{13}C$ values of <38-μm calcites from the DL04 core for the last 6 kyrs.

$CaCO_3$ and the precipitation of Ca and Mg as calcite and/or Mg-calcite.

The $\delta^{18}O$ value of lacustrine endogenic calcite is a function of the $\delta^{18}O$ value and temperature of lake water. An increase of 1‰ in the calcite $\delta^{18}O$ value could be caused either by an increase of 1‰ in the water $\delta^{18}O$ value or by a decrease of 4–5 °C in the water temperature, or by a combination of both, in the equilibrium of oxygen isotopic fractionation (Kim and O'Neil, 1997). Endogenic calcites from the upper 6.39 m of the DL04 core exhibit a large variation of up to 4.1‰ in the $\delta^{18}O$ value (Fig. 4), implying that the water $\delta^{18}O$ played a key role in regulating the calcite $\delta^{18}O$ during the last 6 kyrs. As for closed lakes in semi-arid regions, the water $\delta^{18}O$ is primarily controlled by the evaporative losses of lake water, provided that the source water of precipitation in the region remains essentially unchanged (Ricketts and Johnson, 1996). When evaporation intensifies, more $H_2^{16}O$ would escape from lake water to the atmosphere, leading to the enrichment in ^{18}O of lake water and thus increases in the $\delta^{18}O$ value of endogenic calcites. The $\delta^{18}O$ value of the Dali Lake water is much higher than those of the inflowing river water (Fig. 7; Table 2), suggesting a striking effect of evaporative water losses on the enrichment in ^{18}O of the lake water.

The $\delta^{13}C$ value of lacustrine endogenic calcite is mainly controlled by the $\delta^{13}C_{DIC}$ that is affected by various factors such as $\delta^{13}C$ of the inflowing riverine DIC, primary productivity of the aquatic phytoplankton, burial and degradation of the sedimentary organic matter and isotopic exchange between the lake's DIC and atmospheric CO_2 (Talbot, 1990; Leng and Marshall, 2004). For hydrologically closed, oligotrophic lakes such as Dali Lake, the ^{13}C exchange between the lake's DIC and atmospheric CO_2 could be considered as the dominant factor controlling variations in the $\delta^{13}C_{DIC}$ values of lake water. The degree of such a ^{13}C exchange depends on the residence time and alkalinity of lake water. Under a condition of intensified evaporation in the region, prolonged water residence time and elevated alkalinity would enhance the ^{13}C exchange, resulting in the lake's DIC pool enriched in ^{13}C (Talbot, 1990; Leng and Marshall, 2004). The $\delta^{13}C$ and $\delta^{18}O$ values of endogenic calcites from the DL04 core spanning the last 6 kyrs exhibit a close covariation (Fig. 8), implying that the evaporation of lake water was the common factor that controlled the concentrations of both ^{18}O in the lake water and ^{13}C in the lake's DIC pool (Talbot, 1990).

The above interpretations suggest that significant changes in Ca and Mg concentrations, Mg/Ca ratio and $\delta^{18}O$ and $\delta^{13}C$ values of endogenic calcites from the Dali Lake sediments are all closely related to the intensity of evaporation in the region. Therefore the first factor F1 obtained from PCA of the five geochemical proxies could be used as a proxy indicator for changes in the intensity of evaporation in the region, i.e., an increase in the PCA F1 value indicates intensification in the regional evaporation.

The average data of observations from 1981 to 2010 at Hexigten Banner Meteorological Station, 70 km east of Dali Lake indicate that mean annual evaporation in the Dali Lake region reached its peak value in May when temperature significantly increased but precipitation was relatively lower, and decreased over the months in summer from June–August when both temperature and precipitation were high (Fig. 2). These data indicate that strong evaporation occurring in the region was mainly associated with the balance between temperature and precipitation. High temperature and low precipitation (low effective moisture) were favorable for strong evaporation in the region. However, the observational data exhibit a typical feature of monsoonal climate for the lake region, that was the significant positive relationship between temperature and precipitation and both reached their maximums in summer (Fig. 2). Therefore numerical separation of the relative importance of temperature, precipitation or effective moisture for the evaporation intensity in the region may be not reasonable. On the other hand, historical documents indicate that Dali Lake expanded and lake level rose during the high rainfall years (Li, 1993), and previous studies suggested that increased precipitation input to the lake would decrease the saturation state of calcite (Xiao et al., 2008). In addition, isotopic data of modern meteoric water show that the isotopic fractionation of precipitation in the monsoonal region exhibited significant rainfall effect in summer (Li et al., 2015). Considering all the above influence factors, net losses of water from the lake catchment should dominate the enrichment of elements and isotopes in the lake water and thus in the endogenic calcites. Consequently, significant increases in the PCA F1 value could reflect the occurrence of drought in the region.

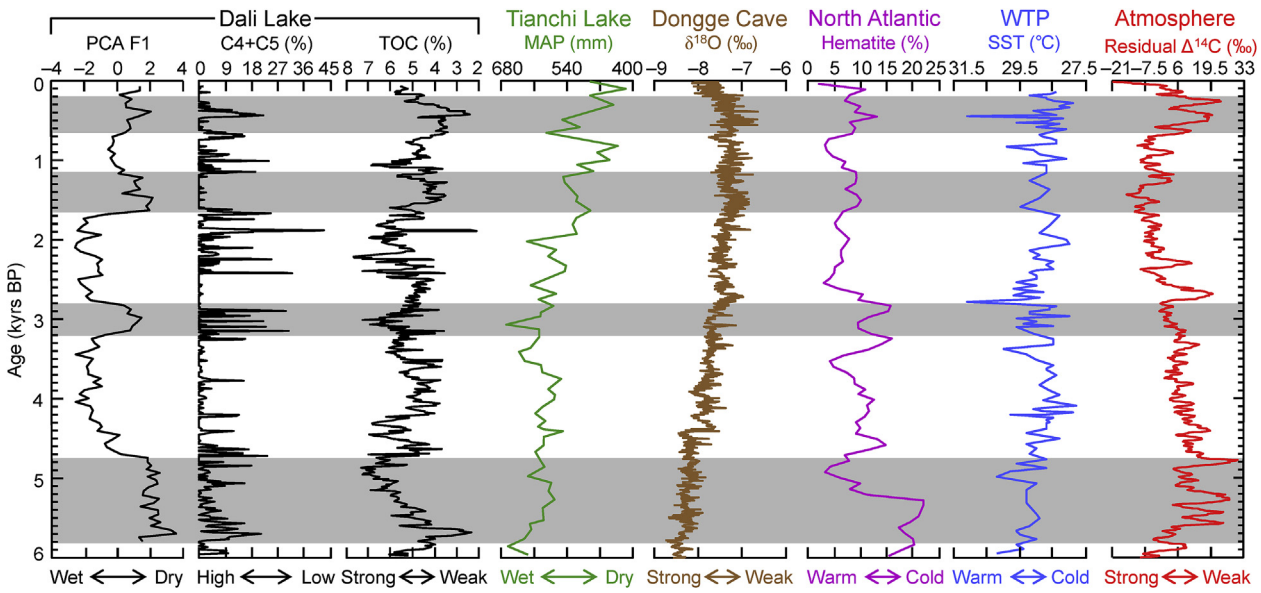

Fig. 9. Correlation of PCA F1 values from the DL04 core spanning the last 6 kyrs with percentages of nearshore suspension and saltation grain size component (C4+C5) (Xiao et al., 2015), total organic carbon (TOC) concentrations (Xiao et al., 2008) from the same sediment core, and with mean annual precipitation (MAP) reconstructed from pollen assemblages from Tianchi Lake (Zhao et al., 2010; Chen et al., 2015) (green curve), oxygen isotopic record of stalagmites from Dongge Cave (Wang et al., 2005) (brown curve), hematite-stained grain concentrations in the North Atlantic sediments (Bond et al., 2001) (pink curve), sea surface temperature (SST) of the western tropical Pacific (WTP) (Stott et al., 2004) (blue curve) and detrended atmospheric residual $\Delta^{14}C$ (Reimer et al., 2013) (red curve). High hematite-stained grain concentration implies high ice-rafted debris and thus cold temperature in the North Atlantic (Bond et al., 2001). High atmospheric residual $\Delta^{14}C$ indicates weak solar activity (Stuiver, 1980). Shaded bars mark the intervals of dry climate in the region. (For interpretation of the references to colour in this figure legend, the reader is referred to the web version of this article.)

5.2. Droughts in the Dali Lake region during the last 6 kyrs

As shown in Fig. 4 and Table 3, the PCA F1 derived from data of Ca and Mg concentrations, Mg/Ca ratio and $\delta^{18}O$ and $\delta^{13}C$ values of the endogenic calcites from the DL04 core exhibits positive values at all the intervals of 5.8–4.75, 3.2–2.8, 1.65–1.15 and 0.65–0.2 kyrs BP. These data indicate that drought occurred in the Dali Lake region at these intervals. It is noticeable that both averages and maximums of the PCA F1 are higher at 5.8–4.75 kyrs BP than at 3.2–2.8, 1.65–1.15 and 0.65–0.2 kyrs BP, implying that the drought occurring at 5.8–4.75 kyrs BP could be the longest-lasting and the most severe one in the region during the last 6 kyrs.

Recent studies on the grain-size distribution of clastic sediments of the DL04 core indicated that the relative percentages of the nearshore suspension and saltation components (C4+C5) increased significantly at the intervals of 5.9–5.35, 3.25–2.85 and 0.7–0.25 kyrs BP for the last 6 kyrs, suggesting large drops in the water level of Dali Lake at these intervals (Xiao et al., 2015) (Fig. 9). Previous studies on the total organic carbon (TOC) concentrations and TOC/TN (C/N) ratios from the same sediment core indicated that TOC concentrations and C/N ratios decreased significantly at 5.9–5.2, 3.2–3.1, 2.9–2.8, 1.5–1.1 and 0.7–0.3 kyrs BP for the last 6 kyrs, implying significant weakening of the surface runoff in the lake catchment (Xiao et al., 2008) (Fig. 9). Despite small difference in the duration between high PCA F1 values and low TOC concentrations at 3.2–2.8 kyrs BP which may be related to the influence of aquatic organic carbon (Fan et al., 2016) (Fig. 9) and despite one inverse relationship between high PCA F1 values and low C4+C5 percentages at 1.65–1.15 kyrs BP which may be induced by the changes in the grain size of source materials (Xiao et al., 2015) (Fig. 9), low lake stands reflected by the high C4+C5 percentages (Xiao et al., 2015) and weak surface runoff implied by the TOC concentrations and C/N ratios (Xiao et al., 2008) generally coincide with the droughts indicated by the geochemical proxies during the last 6 kyrs (Fig. 9), although both grain-size distributions and TOC concentrations and C/N ratios were fully independent of chemical processes occurring in the lake. This coincidence provides substantial support for the PCA-F1-based inference about the droughts occurring in the Dali Lake region during the last 6 kyrs.

The anomalously low $\delta^{18}O$ values of the endogenic calcites at the interval of 5.8–4.75 kyrs BP (Figs. 4 and 7) may be linked to the following two causes. 1) Rapid precipitation of endogenic calcites. Calcite had predominated the precipitation of endogenic carbonates in Dali Lake for the last 6 kyrs; while only at the interval of 5.8–5.4 kyrs BP, did Mg-calcite occur. ^{18}O should be enriched in Mg-calcite relative to calcite (by 0.06‰/mol $MgCO_3$ in calcite) when they were formed under the same conditions (Tarutani et al., 1969; Jiménez-López et al., 2004). Assuming that the carbonates were all $CaCO_3$ at the interval of 5.8–4.75 kyrs BP, then the calculated average $\delta^{18}O$ value was −6.41‰, which was much lower than the original data. Therefore anomalously low $\delta^{18}O$ values at this interval when Mg-calcite occurred should be caused by other factors. The occurrence of Mg-calcite precipitation implies that the precipitation of calcites was accelerated under the super-saturation of $CaCO_3$ in the lake water, thereby resulting in a weakening fractionation of oxygen isotopes between calcites and lake water, and thus decreased $\delta^{18}O$ values of the endogenic calcites (Li et al., 1997; Liu et al., 2009). 2) Inheritance of lake water $\delta^{18}O$. As shown in Fig. 3, $CaCO_3$ contents in bulk samples from the DL04 core are close to zero below the core depth of 6.39 m (5.8 kyrs BP), which implies that Dali Lake had received a large supply of fresh water from the precipitation and the inflowing rivers prior to 5.8 kyrs BP (Xiao et al., 2008). These data denote that $\delta^{18}O$ values of the lake water relatively approximated to those of the precipitation and the riverine water (depleted in ^{18}O) prior to 5.8 kyrs BP. During the following hundreds of yrs after 5.8 kyrs BP, when the regional climate rapidly became dry, the lake water may have remained relatively depleted in ^{18}O, therefore leading to anomalously low $\delta^{18}O$ values of the endogenic calcites.

5.3. Possible causes of the droughts in the EASM margin

Dali Lake is a hydrologically closed lake located at the current northern margin of the EASM (Fig. 1). In the lake, positive balance between inflowing water to the lake and evaporative losses of lake water (the water input to the lake overwhelming the evaporation losses) is closely related to the increases in the monsoonal precipitation in the region on inter-annual and inter-decadal scales (Li, 1993) (Fig. 2), while negative balance (the evaporation losses overwhelming the water input to the lake) may be induced by either decreases in the monsoonal precipitation or increases in the evaporative losses, or a combination of both. However, the coincidence between the drought indicator PCA F1 in this study and the lake level indicator C4+C5 percentages (Xiao et al., 2015) and the surface runoff intensity indicator TOC concentrations (Xiao et al., 2008) from the same sediment core during the last 6 kyrs (Fig. 9) imply that decreases in the monsoonal precipitation may have played a dominant role in triggering the drought events in the region. Decreases in the monsoonal precipitation in the Dali Lake region in the geological past could be indicative of declines in the EASM intensity (An, 2000). Consequently, the regional droughts registered by elements and stable isotopes of the endogenic calcites from Dali Lake at 5.8–4.75, 3.2–2.8, 1.65–1.15 and 0.65–0.2 kyrs BP could imply that the EASM weakened significantly at these 4 intervals (Fig. 9).

The EASM rainfall is the result of the interaction of warm, moist air masses from the low-latitude Pacific with cold, dry airflows from northern high latitudes (An, 2000). In this regard, the EASM intensity and the associated northward penetration of the monsoonal rain belt may be closely related to climatic processes occurring in the western tropical Pacific and in the circum-Arctic regions. It is surprising that large declines in the EASM intensity at the intervals of 5.8–4.75, 3.2–2.8, 1.65–1.15 and 0.65–0.2 kyrs BP coincide, within age uncertainties, very well with the occurrences of ice-rafted debris in the North Atlantic (Bond et al., 2001) but not well with the sea-surface temperature (SST) record from western tropical Pacific (WTP) (Stott et al., 2004) (Fig. 9). These data indicate that the weakening of the EASM at millennial-to-centennial scales was dynamically linked to the cooling of the North Atlantic. In brief, the cooling in the northern high latitudes could generate the low index of the North Atlantic Oscillation and the negative index of Arctic Oscillation, thereby leading to a stronger flow of frigid polar air into the middle latitudes and a southward movement of the circumpolar airflow front (Bond et al., 2001; Shindell et al., 2001; Sung et al., 2006). The intensification of the circumpolar circulation over northern high latitudes could suppress the northward penetration of the EASM circulation (Sung et al., 2006), resulting in significant weakening of the monsoonal precipitation. In addition, the longest and the largest decline in the EASM intensity at 5.8–4.75 kyrs BP for the last 6 kyrs corresponds to the most prominent ice-rafted debris in the North Atlantic for the entire Holocene (Bond et al., 2001) (Fig. 9), providing substantial support for the key role of climatic processes occurring over northern high latitudes in regulating the East Asian monsoon circulation.

Previous studies indicated that the extreme cooling events occurred at ca. 5.5, 4.4, 2.8, 1.6 and 0.5 kyrs BP in the North Atlantic were closely related to the most significant weakening of solar activity during the middle and late Holocene (Bond et al., 2001). Solar forcing could change the surface climate through the atmosphere's dynamic response to changes in stratospheric ozone and temperature (Shindell et al., 2001). In view of the onset and termination as well as the magnitudes, however, there were prominent differences between the cooling events in the North Atlantic and weak solar activity, providing that there were no large dating errors of deep sea sediments. In general, the weak solar activity started at 2.8 kyrs BP significantly lagged behind the corresponding cooling event occurred at ca. 3.2 kyrs BP in the North Atlantic, and the signals of effects of weak solar activity at 4.4 and 1.6 kyrs BP on the surface climate were significantly amplified by the cooling events in the North Atlantic (Bond et al., 2001; Reimer et al., 2013) (Fig. 9). The mechanism for amplifying the solar signals may be related to the surface hydrographic changes (Bond et al., 2001). As seen in Figure 9, the significant weakening of the EASM recorded by the proxy indicators from Dali Lake during the last 6 kyrs do not match very well with the prominently reduced solar activity (Reimer et al., 2013). It seems that only at two intervals, 5.65–5.15 and 0.7–0.2 kyrs BP, is there a consistency between them (Fig. 9). These data indicate that solar activity may partly, but not mainly, be responsible for the EASM variability. Solar activity may influence the East Asian monsoon circulation through changing surface winds and surface ocean hydrography in the North Atlantic, which may have affected the production rate of North Atlantic Deep Water, potentially providing a mechanism of amplifying the solar impacts on the cooling in the North Atlantic (Bond et al., 2001).

Regional comparison between the proxy indicators from Dali Lake (43°15.68′ N, 116°36.26′ E) and the mean annual precipitation (MAP) reconstructed from pollen assemblages from Tianchi Lake (35°15.88′ N, 106°18.55′ E) (Zhao et al., 2010; Chen et al., 2015) and the oxygen isotopic record of stalagmites from Dongge Cave (25°17′ N, 108°5′ E) (Wang et al., 2005) in the monsoonal region during the last 6 kyrs (Figs. 1 and 9) exhibits significant differences in both the variation trends on millennial scales and the magnitudes on centennial scales. On millennial scales, a gradual weakening trend of the Asian monsoon intensity was implied from the gradual decreases in the MAP from Tianchi Lake (Zhao et al., 2010) and increases in the $\delta^{18}O$ values of stalagmites from Dongge Cave (Wang et al., 2005) in the relatively lower latitudes, which is absent in the records from Dali Lake in northern China (Figs. 1 and 9). However, the gradual weakening of the Asian summer monsoon during the last 6 kyrs recorded in the lower latitudes correlates well with the gradual decreases in the SST of WTP (Stott et al., 2004) (Fig. 9), implying that the cooling of WTP (which may be caused by the gradual decreases in the Northern Hemisphere summer insolation, e.g., An, 2000) may have played an important role in regulating the Asian summer monsoon intensity in the lower latitudes. On centennial scales, the events of weak Asian monsoon intensity indicated by the records from both Tianchi Lake (Zhao et al., 2010) and Dongge Cave (Wang et al., 2005) are not so prominent as those recorded from Dali Lake in northern China within age uncertainties (Figs. 1 and 9). The larger magnitudes of declines in the EASM intensity in the relatively higher latitudes are supported by the TOC and $\delta^{13}C_{TOC}$ records of wetland sediments from Gimpo in central Korea (37°32′ N, 126°48′ E) (Lim et al., 2015). The striking contrasts of the weak monsoon intensity between high and low latitudes may indicate that the influence of the North Atlantic cooling on the Asian monsoon intensity generally decreased with the decreases in the latitudes (Figs. 1 and 9). Alternatively, the Asian monsoon intensity in the lower latitudes may be influenced by the cooling events in the North Atlantic through surface hydrographic changes rather than atmosphere's dynamic changes (Wang et al., 2005, 2008; Chen et al., 2016) or by some other driving forces such as El Niño Southern Oscillation (Selvaraj et al., 2012) and Walker Circulation variations (Yan et al., 2011) in the tropical Pacific. In addition, the events of weak Asian monsoon intensity in the lower latitudes during the last 6 kyrs correlate not very well with those of weak solar activity (Fig. 9), which provides additional insights that solar activity may have triggered the monsoon variability, but not been responsible for the feedback process in the climate system.

It is notable that the drought occurring in the Dali Lake region at 5.8–4.75 kyrs BP terminated ca. 500 yrs later than the

corresponding cooling event in the North Atlantic (Bond et al., 2001) (Fig. 9). We infer that this time lag may result from a decrease in the sensitivity of carbonate precipitation within the lake to short-scale significant climate changes, due to the shift of the lake's hydrochemical state. In other words, when the lake experienced a shift from Mg-calcite precipitation (occurring in the former 500 yrs at the interval of 5.8–4.75 kyrs BP) to calcite precipitation (occurring in the latter 500 yrs at the interval of 5.8–4.75 kyrs BP), an abrupt decrease in the aridity of the region may not be able to cause a rapid and significant reduction in the residence time of solutes and isotopes in the lake water, so that the calcite precipitation within the lake could not respond immediately to the dry–wet fluctuations in the regional climate. Moreover, the North Atlantic cooling at ca. 4.4–3.9 kyrs BP (Bond et al., 2001) had not been recorded by the elements and stable isotopes of the endogenic calcites from Dali Lake sediments (Fig. 9), which may be related either to the instability of the short-scale feedback process and signal propagation between climatic sub-systems or to the complexity of the lake–catchment system of Dali Lake.

6. Conclusions

Carbonates finer in grain size than 38 μm from the core sediments of Dali Lake in central-eastern Inner Mongolia were predominated by endogenic calcites precipitated within the water body of the lake. Increases in the values of Ca and Mg concentrations, Mg/Ca ratio, $\delta^{18}O$ and $\delta^{13}C$ of the endogenic calcites are interpreted to reflect more evaporative losses of lake water than water input to the lake and thus drought events in the region. The chemical proxy data in this study combined with multi-proxy indicators including grain size component and TOC concentrations from the same sediment core imply that declines in the EASM intensity may have played a dominant role in triggering the drought events during the last 6 kyrs. The elemental and stable isotopic records of endogenic calcites from the upper 6.39 m of the DL04 core indicate that the EASM largely weakened at the intervals of 5.8–4.75, 3.2–2.8, 1.65–1.15 and 0.65–0.2 kyrs BP for the last 6 kyrs. Large declines in the EASM intensity during the last 6 kyrs correspond in time to occurrences of ice-rafted debris in the North Atlantic, indicating that millennial-to-centennial scale changes in the EASM intensity were mainly controlled by climatic processes occurring in the northern high latitudes. These data suggest that the EASM may intensify and thus bring more rainfall to the semi-arid regions of northern China under the condition of persistent global warming on sub-millennial scales.

Acknowledgements

The authors are grateful to the editor Neil Roberts and two anonymous reviewers for constructive comments and suggestions to this manuscript. This work is supported by the National Natural Science Foundation of China (Grant 41130101) and the Ministry of Science and Technology of China (Grant 2010CB833400).

References

An, Z.S., 2000. The history and variability of the East Asian paleomonsoon climate. Quat. Sci. Rev. 19, 171–187.
Bond, G., Kromer, B., Beer, J., Muscheler, R., Evans, M.N., Showers, W., Hoffmann, S., Lotti-Bond, R., Hajdas, I., Bonani, G., 2001. Persistent solar influence in north Atlantic climate during the Holocene. Science 294, 2130–2136.
Broecker, W.S., Putnam, A.E., 2013. Hydrologic impacts of past shifts of Earth's thermal equator offer insight into those to be produced by fossil fuel CO_2. Proc. Natl. Acad. Sci. U. S. A. 110, 16710–16715.
Bronk Ramsey, C., Lee, S., 2013. Recent and planned developments of the program OxCal. Radiocarbon 55, 720–730.
Camberlin, P., Janicot, S., Poccard, I., 2001. Seasonality and atmospheric dynamics of the teleconnection between African rainfall and tropical sea-surface temperature: Atlantic VS. ENSO. Int. J. Climatol. 21, 973–1005.
Chen, F.H., Xu, Q.H., Chen, J.H., Birks, H.J.B., Liu, J.B., Zhang, S.R., Jin, L.Y., An, C.B., Telford, R.J., Cao, X.Y., Wang, Z.L., Zhang, X.J., Selvaraj, K., Lu, H.Y., Li, Y.C., Zheng, Z., Wang, H.P., Zhou, A.F., Dong, G.H., Zhang, J.W., Huang, X.Z., Bloemendal, J., Rao, Z.G., 2015. East Asian summer monsoon precipitation variability since the last deglaciation. Sci. Rep. 5, 11186. http://dx.doi.org/10.1038/srep11186.
Chen, H., Edwards, R.L., Sinha, A., Spötl, C., Yi, L., Chen, S.T., Kelly, M., Kathayat, G., Wang, X.F., Li, X.L., Kong, X.G., Wang, Y.J., Ning, Y.F., Zhang, H.W., 2016. The Asian monsoon over the past 640,000 years and ice age terminations. Nature 534, 640–646.
Eugster, H.P., Jones, B.F., 1979. Behavior of major solutes during closed-basin brine evolution. Am. J. Sci. 279, 609–631.
Fan, J.W., Xiao, J.L., Wen, R.L., Zhang, S.R., Wang, X., Cui, L.L., Yamagata, H., 2016. Carbon and nitrogen signatures of sedimentary organic matter from Dali Lake in Inner Mongolia: implications for Holocene hydrological and ecological variations in the East Asian summer monsoon margin. Quat. Int. under review.
Fontes, J.Ch, Gasse, F., Gibert, E., 1996. Holocene environmental changes in Lake Bangong Basin (Western Tibet). Part 1: chronology and stable isotopes of carbonates of a Holocene lacustrine core. Palaeogeogr. Palaeoclimatol. Palaeoecol. 120, 25–47.
Gu, Z.Y., Liu, J.Q., Yuan, B.Y., Liu, T.S., Liu, R.M., Liu, Y., Yaskawa, K., 1993. Monsoon variations of the Qinghai-Xizang plateau during the last 12,000 years—Geochemical evidence from the sediments in the Siling lake. Chin. Sci. Bull. 38, 577–581.
Held, I.M., Soden, B.J., 2006. Robust responses of the hydrological cycle to global warming. J. Clim. 19, 5686–5699.
IPCC, 2013. Climate Change 2013: The Physical Science Basis. Contribution of Working Group I to the Fifth Assessment Report of the Intergovernmental Panel on Climate Change. In: T.F., Stocker, Qin, D., Plattner, G.K., Tignor, M., Allen, S.K., Boschung, J., Nauels, A., Xia, Y., Bex, V., Midgley, P.M. (Eds.). Cambridge University Press, United Kingdom and New York, NY, USA, p. 1535.
Ito, E., Forester, R.M., 2009. Changes in continental ostracode shell chemistry: uncertainty of cause. Hydrobiologia 620, 1–15.
Jiang, W.Y., Liu, T.S., 2007. Timing and spatial distribution of mid-Holocene drying over northern China: response to a southeastward retreat of the East Asian Monsoon. J. Geophys. Res. 112, D24111. http://dx.doi.org/10.1029/2007JD009050.
Jiménez-López, C., Romanek, C.S., Huertas, F.J., Ohmoto, H., Caballero, E., 2004. Oxygen isotope fractionation in synthetic magnesian calcite. Geochimica Cosmochimica Acta 68, 3367–3377.
Kim, S.T., O'Neil, J.R., 1997. Equilibrium and nonequilibrium oxygen isotope effects in synthetic carbonates. Geochimica Cosmochimica Acta 61, 3461–3475.
Leng, M.J., Marshall, J.D., 2004. Palaeoclimate interpretation of stable isotope data from lake sediment archives. Quat. Sci. Rev. 23, 811–831.
Lerman, A., 1978. Lakes: Chemistry, Geology, Physics. Springer, 363 pp.
Lerman, A., 1979. Geochemical Processes: Water and Sediment Environments. Wiley, New York.
Li, H.-C., Stott, L.D., Hammond, D.E., 1997. Temperature and salinity effects on ^{18}O fractionation for rapidly precipitated carbonates: laboratory experiments with alkaline lake water. Episodes 20, 193–198.
Li, J., Tao, T., Pang, Z.H., Tan, M., Kong, Y.L., Duan, W.H., Zhang, Y.W., 2015. Identification of different moisture sources through isotopic monitoring during a storm event. J. Hydrometeorol. 16, 1918–1927.
Li, J.P., Wu, Z.W., Jiang, Z.H., He, J.H., 2010. Can global warming strengthen the East Asian summer monsoon? J. Clim. 23, 6696–6705.
Li, Z.G., 1993. Annals of Hexigten Banner. People's Press of Inner Mongolia, Hohhot, 1144 pp (in Chinese).
Lim, J., Yang, D.-Y., Lee, J.-Y., Hong, S.-S., Um, I.K., 2015. Middle Holocene environmental change in central Korea and its linkage to summer and winter monsoon changes. Quat. Res. 84, 37–45.
Liu, W.G., Li, X.Z., Zhang, L., An, Z.S., Xu, L.M., 2009. Evaluation of oxygen isotopes in carbonate as an indicator of lake evolution in arid areas: the modern Qinghai Lake, Qinghai–Tibet Plateau. Chem. Geol. 268, 126–136.
Lohmann, G., 2003. Atmospheric and oceanic freshwater transport during weak Atlantic overturning circulation. Tellus 55A, 438–449.
Müller, G., Irion, G., Förstner, U., 1972. Formation and diagenesis of inorganic Ca-Mg carbonates in the lacustrine environment. Naturwissenschaften 59, 158–164.
Nakamura, T., Niu, E., Oda, H., Ikeda, A., Minami, M., Takahashi, H., Adachi, M., Pals, L., Gottdang, A., Suya, N., 2000. The HVEE Tandetron AMS system at Nagoya University. Nucl. Instrum. Methods Phys. Res. B172, 52–57.
Nelson, D.B., Abbott, M.B., Steinman, B., Polissar, P.J., Stansell, N.D., Ortiz, J.D., Rosenmeier, M.F., Finney, B.P., Riedel, J., 2011. Drought variability in the Pacific Northwest from a 6,000-yr lake sediment record. Proc. Natl. Acad. Sci. U. S. A. 108, 3870–3875.
Qiang, M.R., Chen, F.H., Zhang, J.W., Gao, S.Y., Zhou, A.F., 2005. Climatic changes documented by stable isotopes of sedimentary carbonate in Lake Sugan, northeastern Tibetan Plateau of China, since 2 ka BP. Chin. Sci. Bull. 50, 1930–1939.
Reimer, P.J., Bard, E., Bayliss, A., Beck, J.W., Blackwell, P.G., Bronk Ramsey, C., Buck, C.E., Cheng, H., Edwards, R.L., Friedrich, M., Grootes, P.M., Guilderson, T.P., Haflidason, H., Hajdas, I., Hatté, C., Heaton, T.J., Hoffmann, D.L., Hogg, A.G., Hughen, K.A., Kaiser, K.F., Kromer, B., Manning, S.W., Niu, M., Reimer, R.W., Richards, D.A., Scott, E.M., Southon, J.R., Staff, R.A., Turney, C.S.M., van der

Plicht, J., 2013. INTCAL13 and MARINE13 radiocarbon age calibration curves, 0-50,000 years cal BP. Radiocarbon 55, 1869–1887.
Ricketts, R.D., Johnson, T.C., 1996. Climate change in the Turkana basin as deduced from a 4000 year long $\delta^{18}O$ record. Earth Planet. Sci. Lett. 142, 7–17.
Russell, J.M., Johnson, T.C., 2005. Late Holocene climate change in the north Atlantic and equatorial Africa: millennial-scale ITCZ migration. Geophys. Res. Lett. 32, L17705. http://dx.doi.org/10.1029/2005GL023295.
Russell, J.M., Johnson, T.C., Talbot, M.R., 2003. A 725 yr cycle in the climate of central Africa during the late Holocene. Geology 31, 677–680.
Selvaraj, K., Wei, K.Y., Liu, K.K., Kao, S.J., 2012. Late Holocene monsoon climate of northeastern Taiwan inferred from elemental (C, N) and isotopic ($\delta^{13}C$, $\delta^{15}N$) data in lake sediments. Quat. Sci. Rev. 37, 48–60.
Shindell, D.T., Schmidt, G.A., Mann, M.E., Rind, D., Waple, A., 2001. Solar forcing of regional climate change during the Maunder Minimum. Science 294, 2149–2152.
Staubwasser, M., Sirocko, F., Grootes, P.M., Segl, M., 2003. Climate change at the 4.2 ka BP termination of the Indus valley civilization and Holocene south Asian monsoon variability. Geophys. Res. Lett. 30, 1425. http://dx.doi.org/10.1029/2002GL016822.
Steinman, B.A., Pompeani, D.P., Abbott, M.B., Ortiz, J.D., Stansell, N.D., Finkenbinder, M.S., Mihindukulasooriya, L.N., Hillman, A.L., 2016. Oxygen isotope records of Holocene climate variability in the Pacific Northwest. Quat. Sci. Rev. 142, 40–60.
Stott, L., Cannariato, K., Thunell, R., Haug, G.H., Koutavas, A., Lund, S., 2004. Decline of surface temperature and salinity in the western tropical Pacific Ocean in the Holocene epoch. Nature 431, 56–59.
Stuiver, M., 1980. Solar variability and climatic change during the current millennium. Nature 286, 868–871.
Sung, M.-K., Kwon, W.-T., Baek, H.-J., Boo, K.-O., Lim, G.-H., Kug, J.-S., 2006. A possible impact of the North Atlantic Oscillation on the east Asian summer monsoon precipitation. Geophys. Res. Lett. 33, L21713. http://dx.doi.org/10.1029/2006GL027253.
Talbot, M.R., 1990. A review of the palaeohydrological interpretation of carbon and oxygen isotopic ratios in primary lacustrine carbonates. Chem. Geol. 80, 261–279.
Talbot, M.R., Allen, P.A., 1996. Lakes. In: Reading, H.G. (Ed.), Sedimentary Environments: Processes, Facies and Stratigraphy. Blackwell Publishing, Oxford.
Tarutani, T., Clayton, R.N., Mayeda, T.K., 1969. The effect of polymorphism and magnesium substitution on oxygen isotope fractionation between calcium carbonate and water. Geochimica Cosmochimica Acta 33, 987–996.
Vellinga, M., Wood, R.A., 2002. Global climatic impacts of a collapse of the Atlantic thermohaline circulation. Clim. Change 54, 251–267.
Wang, Y.J., Cheng, H., Edwards, R.L., He, Y.Q., Kong, X.G., An, Z.S., Wu, J.Y., Kelly, M.J., Dykoski, C.A., Li, X.D., 2005. The Holocene Asian monsoon: links to solar changes and North Atlantic climate. Science 308, 854–857.
Wang, Y.J., Cheng, H., Edwards, R.L., Kong, X.G., Shao, X.H., Chen, S.T., Wu, J.Y., Jiang, X.Y., Wang, X.F., An, Z.S., 2008. Millennial- and orbital-scale changes in the East Asian monsoon over the past 224,000 years. Nature 451, 1090–1093.
Xiao, J.L., Fan, J.W., Zhai, D.Y., Wen, R.L., Qin, X.G., 2015. Testing the model for linking grain-size component to lake level status of modern clastic lakes. Quat. Int. 355, 34–43.
Xiao, J.L., Si, B., Zhai, D.Y., Itoh, S., Lomtatidze, Z., 2008. Hydrology of Dali Lake in central-eastern inner Mongolia and Holocene East Asian monsoon variability. J. Paleolimnol. 40, 519–528.
Yan, H., Sun, L.G., Oppo, D.W., Wang, Y.H., Liu, Z.H., Xie, Z.Q., Liu, X.D., Cheng, W.H., 2011. South China Sea hydrological changes and Pacific Walker Circulation variations over the last millennium. Nat. Commun. 2, 293. http://dx.doi.org/10.1038/ncomms1297.
Yu, Z.C., Ito, E., 1999. Possible solar forcing of century-scale drought frequency in the northern Great Plains. Geology 27, 263–266.
Zhao, Y., Chen, F.H., Zhou, A.F., Yu, Z.C., Zhang, K., 2010. Vegetation history, climate change and human activities over the last 6200 years on the Liupan Mountains in the southwestern Loess Plateau in central China. Palaeogeogr. Palaeoclimatol. Palaeoecol. 293, 197–205.